COBEM 2021 26th International Congress of Mechanical Engineering
November 22-26, 2021, Virtual Congress, Brazil
ABCM Associação Brasileira de Engenharia e Ciências Mecânicas

COBEM2021-1728
NUMERICAL EXPERIMENTS OF COMPRESSIBLE FLOW USING THE MULTI DIRECT FORCING

Rafael Romão da Silva Melo
Department of Thermal Science and Fluids, Federal University of São João del-Rei, 170 Frei Orlando Square, São João del-Rei, Brazil
rafaelmelo@ufsj.edu.br

Alessandra Ribeiro da Silva
Aristeu da Silveira Neto
Fluid Mechanics Laboratory, Federal University of Uberlândia, 2121 Av. João Naves de Ávila, Uberlândia, Brazil
alessandra.silva@ufu.br
aristeus@ufu.br

Abstract. *This present work presents the numerical experiments of compressible flow using the immersed boundary method with the multi direct forcing technic. Cartesian numerical meshes are used for non-Cartesian problems thanks to the dynamic immersed boundary method. All the implementations and simulations are carried out using an in-house computational code MFSim (Multiphysics Simulator), which allows to solve the Navier-Stokes equations in the transient three-dimensional form using block-structured mesh with local adaptability. Three cases were performed in the validation: the reflection of a shock wave in a flat plate, compressible flow over an inclined plate, and compressible flow around a cylinder. Consistent qualitative results are obtained, and corresponding quantitative results compare well with the reference results that other authors have published.*

Keywords: *Compressible flow, Immersed Boundary Method, Adaptive mesh refinement*

1. INTRODUCTION

Many scientific and practical applications involve flows, where there are regions which is compressible and other areas where fluid compressibility is minimal or non-existent. Thus, it is necessary to study and implement numerical techniques that solve incompressible or compressible flows depending on the flow characteristic. These techniques that encompass all regimes, from incompressible to supersonic, are known as *All-Mach* Techniques, or techniques that solve the flow at any speed (Maliska, 1995).

The use of Cartesian grid limits the application of the methodology to the solution of simple problems. One solution to this problem is the use of the immersed boundary method. The boundary conditions are applied indirectly (Melo *et al.*, 2020). Two grids are used, an Eulerian one for the fluid and the other one, Lagrangian, for the immersed boundary.

This present work presents the numerical experiments of compressible flow using the immersed boundary method with the multi direct forcing technic. All the implementations and simulations are carried out using an in-house computational code MFSim (Multiphysics Simulator), which allows to solve the Navier-Stokes equations in the transient three-dimensional form using block-structured mesh.

2. MATHEMATICAL MODEL

In this section, the partial differential equations that model the problem along with the boundary conditions and initial conditions are presented, when applicable.

2.1 Eulerian domain

In all simulated cases, compressible flows of Newtonian fluids are considered. The equation of the mass balance for the case of compressible flow in Cartesian coordinates, using the index notation is given by Eq. (1).

$$\frac{\partial \rho}{\partial t} + \frac{\partial \rho u_j}{\partial x_j} = 0, \quad j = 1, 2, 3, \tag{1}$$

where ρ is the specific mass, t the time variable, u_j is the fluid velocity component in j direction and x_j are the Cartesian coordinates directions x, y and z, respectively. Equation (2) represents the balance of the momentum, written in divergent

form, in Cartesian coordinates and in indicial notation.

$$\frac{\partial \rho u_i}{\partial t} + \frac{\partial \rho u_i u_j}{\partial x_j} = -\frac{\partial p}{\partial x_i} + \frac{\partial}{\partial x_j}\left[\mu\left(\frac{\partial u_i}{\partial x_j} + \frac{\partial u_j}{\partial x_i}\right) - \frac{2}{3}\mu\left(\frac{\partial u_k}{\partial x_k}\right)\delta_{i,j}\right], \tag{2}$$

where $i, j = 1, 2, 3$, p is the pressure, t is the time, and δ defined as the Kronecker operator.

Equation (3) represents the thermal energy balance for a Newtonian fluid, written in divergent form, in Cartesian coordinates and in indicial notation.

$$\frac{\partial(\rho c_p T)}{\partial t} + \frac{\partial\left(\rho c_p T u_i\right)}{\partial x_i} = \frac{\partial}{\partial x_i}\left(k\frac{\partial T}{\partial x_i}\right) + \Phi + \lambda \tag{3}$$

where i, j and $k = 1, 2, 3$, c_p is the specific heat at constant pressure and Φ and λ are given by Eqs. (4) and (5), respectively.

$$\Phi = \mu\left[\left(\frac{\partial u_i}{\partial x_j} + \frac{\partial u_j}{\partial x_i}\right)^2 + \left(\frac{\partial u_i}{\partial x_k} + \frac{\partial u_k}{\partial x_i}\right)^2 + \left(\frac{\partial u_j}{\partial x_k} + \frac{\partial u_k}{\partial x_j}\right)^2 + 2\left(\frac{\partial u_i}{\partial x_i}\right)^2\right] - \frac{2}{3}\mu\left(\frac{\partial u_i}{\partial x_i}\right)^2 \tag{4}$$

$$\lambda = \frac{\partial p}{\partial t} + u_i\frac{\partial p}{\partial x_i} \tag{5}$$

In the present work, the SIMPLE (Semi-Implicit Method for Pressure Linked Equations) method developed by Patankar and Spalding (1983) was used in a Cartesian and staggered grid. In this method the equations for the correction of velocities are obtained by from the momentum equations and mass balance equation. For more details, see Ferziger and Peric (2012).

2.2 *All-Mach* methodology

Few numerical methods apply to both incompressible and compressible flows. The scientific community's effort to seek general ways to solve flows for any Mach number began in the late 1960s. Pioneering work in this line was by the authors Harlow and Amsden (1968) who proposed a technique, called ICE, to the solution of transient problems contemplating an extensive range of the Mach number.

More recently, Darwish (2000) have reformulated the SIMPLE's family using a co-located mesh approach to predict single fluid flows at any Mach number. Furthermore, the philosophies behind these algorithms, as well as their similarities and differences, are explained. Later, Darwish and Moukalled (2014) extended these reformulations, mentioned above, to the case of flows with more than one fluid. Darwish *et al.* (2007, 2009) also presented a fully coupled method for incompressible flows and in a recent work Darwish and Moukalled (2014) extended this fully coupled algorithm to situations involving compressible flows.

The main idea for creating an *All-mach* solver is the deduction of an equation for the pressure fluctuation that takes into account the density variation due to the fluid's compressibility. For this, we started from the equation of complete continuity and linearized the specific mass-velocity product as follows:

$$\rho u_i = \rho' {u_i}^* + \rho^* {u_i}' - \rho^* {u_i}^*, \tag{6}$$

where ρ^* and ${u_i}^*$ are the specific mass and estimated velocities in this iteration (Maliska, 1995)

The term u_i' brings the contribution of the pressure fluctuation of the *momentum* equation:

$${u_i}' = {u_i}^* - \frac{1}{A_{pU_i}}\frac{\partial p'}{\partial x_i}. \tag{7}$$

And the term ρ' brings the contribution of density variation due to pressure variation (fluctuation), which the equation of state can model:

$$\rho' = \frac{p'}{RT}, \tag{8}$$

where p' is the pressure fluctuation, R is the universal gas constant, and T is the fluid temperature.

Combining the Eqs. 6, 7 and 8 with the continuity equation for a compressible fluid (Eq. 1), we obtain an equation for the pressure fluctuation that operates in the most distinct Mach numbers, being able to simulate incompressible, subsonic, transonic, and even supersonic flows (Ferziger and Peric, 2012; Maliska, 1995).

2.3 The immersed boundary formulation

A Lagrangian mesh is used to represent the immersed boundary, which models a body immersed within the fluid flow. One of the main advantages of the immersed boundary method is that it is possible to represent a complex and mobile body inside the flow even when a cartesian mesh is used. In the present work, the multi direct forcing (MDF) method, based on the work of Wang *et al.* (2008), was used.

A Eulerian forcing field, $f_i(x,t)$, is used to modeling the influence of solid boundary over any neighboring fluid particle placed at the position $\vec{x}$. The linear momentum balance for the fluid particle $\vec{x}$ is given by Equation (2), that can be rewritten as follows:

$$\frac{\partial u_i(\vec{x},t)}{\partial t} = RHS_i(\vec{x},t) + \frac{1}{\rho} f_i(\vec{x},t). \tag{9}$$

To model the forcing term $f_i(x,t)$, the transient term of Equation (9) is discretized using a first-order Euler method. This first-order scheme was only used here to illustrate the development of the dynamic forcing model. The dicretized equation will be decomposed in the following two equations:

$$\frac{u_i^*(\vec{x},t) - u_i^n(\vec{x},t)}{\Delta t} = RHS_i^n(\vec{x},t) \tag{10}$$

and

$$f_i^{n+1}(\vec{x},t) = \rho \frac{\widetilde{u}_i^{n+1}(\vec{x},t) - u_i^*(\vec{x},t)}{\Delta t}, \tag{11}$$

where $n+1$ is the current time step and $\widetilde{u}_i^{n+1}$ is the velocity of a fluid particle placed near the solid interface under the influence of the forcing field. For convenience, the term $u_i^*(\vec{x},t)$, which is the guess velocity, was added and subtracted the discretized equation.

Although the velocity $\widetilde{u}_i^{n+1}(\vec{x},t)$ for a fluid particle is not given, the velocity of the solid interface is generally known. Therefore, Equation (11) is rewritten for the fluid's particles $\vec{x}_k$ that are placed near to the solid surface:

$$F_i^{n+1}(\vec{x}_k,t) = \rho \frac{\widetilde{U}_i^{n+1}(\vec{x}_k,t) - U_i^*(\vec{x}_k,t)}{\Delta t} \tag{12}$$

where $F_i^{n+1}(\vec{x}_k,t)$ is the Lagrangian force that the surface exerts over the particle $\vec{x}_k$, forcing these particles to have the same velocity $\widetilde{U}_i^{n+1}(\vec{x}_k,t)$ of the solid surface. The Lagrangian velocity $U_i^*(\vec{x}_k,t)$ of a particle placed close to the solid surface is obtained by the interpolation of the Eulerian velocity estimation $u_i^*(\vec{x},t)$ as given by Equation (13):

$$U_i^*(\vec{x}_k,t) = \sum_{\Omega} u_i^*(\vec{x},t)\, D_h(\vec{x} - \vec{x}_k)\, h^3. \tag{13}$$

In Equation (13), the summation must be performed over the Eulerian domain, Ω, using a compact support Dirac Kernel, $D_h(\vec{x} - \vec{x}_k)$. Equation (12) provides a measure of the velocity difference between a fluid particle that is placed at the surface and the velocity of the surface itself. This difference is converted into a Lagrangian force. The Lagrangian force calculated using Equation (12) can be distributed from the Lagrangian domain Γ to the Eulerian domain Ω:

$$f_i^{n+1}(\vec{x},t) = \sum_{\Gamma} F_i^{n+1}(\vec{x}_k,t)\, D_h(\vec{x} - \vec{x}_k)\, h^3. \tag{14}$$

Because the Eulerian force field, $f_i^{n+1}(\vec{x},t)$ $[N/m^3]$, is evaluated through Equation (14), the velocity can be calculated, using Equation (15):

$$\widetilde{u}_i^{n+1}(\vec{x},t) = u_i^*(\vec{x},t) + \frac{\Delta t}{\rho} f_i^{n+1}(\vec{x},t). \tag{15}$$

The multi-forcing process is performed using Equations (12) to (15) to achieve a required tolerance. This convergence is verified using a L_2 norm that is calculated by a summation over all of the Lagrangian points.

3. RESULTS AND DISCUSSION

We perform simulations of four cases to validate the immersed boundary method with compressible flows: oblique shock on a flat plate, shock on an inclined plate, supersonic flow on an ascending step, and supersonic flow on a cylinder.

3.1 Oblique shock wave on a flat plate

In the first case, to validate the implementations, we simulate the case of the oblique shock on a flat plate, described in the Figure (1). In this case, three supersonic boundary conditions are imposed, one at the west entrance of the domain, with Mach number $Ma = 2.9$, the other at the top of the domain, with Mach $Ma = 2,378$, and the last one in the output, with Mach $Ma = 1,942$. In this same figure, the analytical solution is outlined, with the shock wave angulation and the position of the reflection being presented. A two-dimensional case was set with the domain of $4.1\ m$ in x and $1.0\ m$ in y. A mesh with a resolution of 160 volumes in the x direction was used.

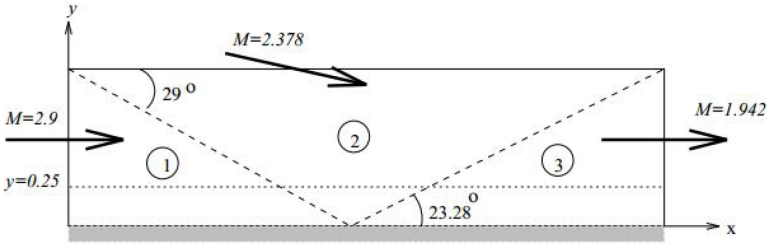

Figure 1. Setup of the oblique shock case on a flat plate.

For comparison, two cases were configured in MFSim: the first using conventional boundary condition and the second modeling the flat plate with immersed boundary. As the methodology demands a complementary flow region, increasing the domain in the y direction is below the flat plate. Fig. (2) presents the specific mass fields for the two cases, and in the region of interest, the flows are qualitatively similar. In the complementary region of the case with immersed boundary, we saw a small reflection near the exit, which does not influence the solution.

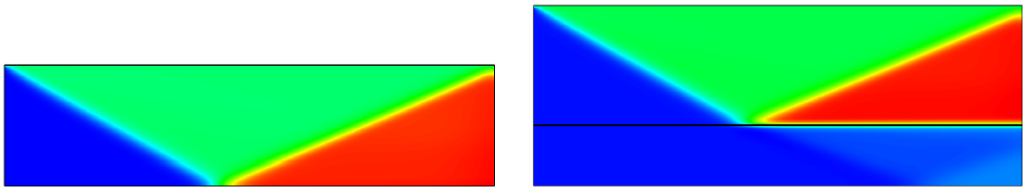

(a) Traditional boundary condition (b) Immersed boundary method

Figure 2. Comparison of the shock wave reflected on a flat plate.

The Figure (3) presents a comparison of the specific mass solutions for the two previous cases with the analytical solution in the position $y = 0.25\ m$. Both solutions, with conventional boundary conditions and immersed boundary method, are similar to the analytical solution.

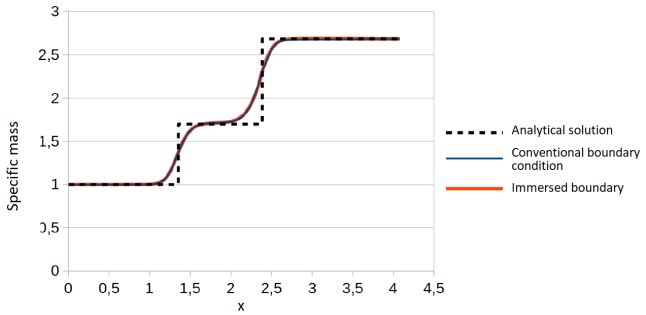

Figure 3. Comparison of specific mass with analytical solution for both cases.

To improve the results, we simulated a case with twice as much refinement. The figure (4) presents the solution of the specific mass along x at $y = 0.25\ m$. Note that with the refinement, there was an approximation of the result with the analytical solution.

For a simple flat plate, the methodology was validated. So we started to validate a second case, the inclined flat plate.

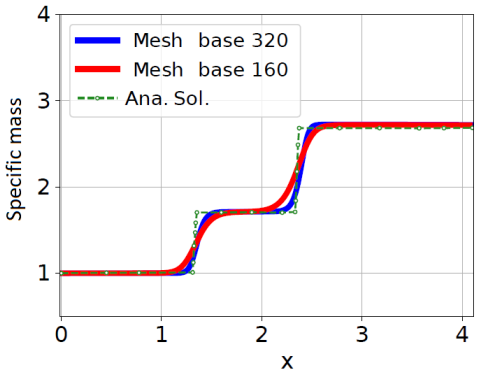

Figure 4. Comparison of specific mass with analytical solution for the two refinements.

3.2 Shock wave on an inclined plate

For the second validation, we performed the flow simulation over an inclined plate, based on the work of Xiao *et al.* (2017). The figure (5) presents a scheme of the case, where an initial position of the shock wave close to the inclined plate is defined. The fluid properties are chosen in such a way that in the initial condition, the Mach number before the shock is 1.7 and after the shock is 0.0. An immersed boundary models the inclined plate, and the simulation domain has dimensions of $0.8\ m$ in x and $0.5\ m$ in y. The mesh resolution is 256 volumes in x and 160 volumes in y.

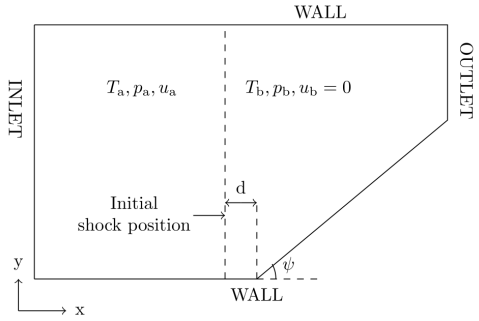

Figure 5. Setup of the shock wave on an inclined plate.

The figure (6) presents the Mach field obtained with the present simulation compared to the reference data. Note the consistency of the obtained solution. There is a region of high Mach in front of the shock wave, a region with a relatively low Mach value at the beginning of the plate, in minimum value of y. It is also possible to observe the consistency in the expansion wave in the direction perpendicular to the immersed boundary. The flow in the complementary region does not affect the solution in the interest domain.

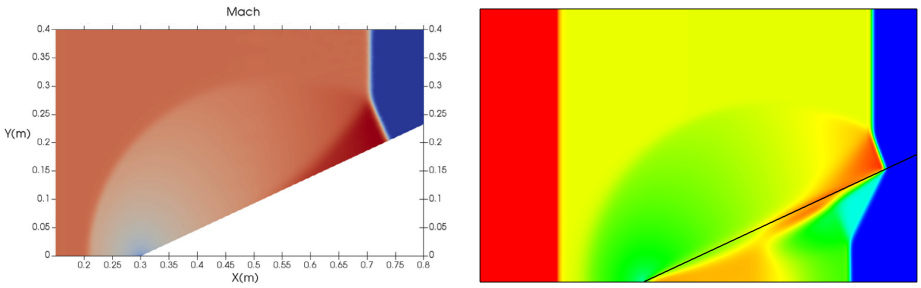

(a) Xiao *et al.* (2017) (b) Present work

Figure 6. Mach field.

The figure (7) shows the specific mass for this case. It is also possible to notice the consistency of our results when comparing them with reference data. It is possible to observe a region with a high specific mass value between the shock wave and the expansion wave.

Next, results for the third case will be presented for validation of the immersed boundary method with compressibility effects.

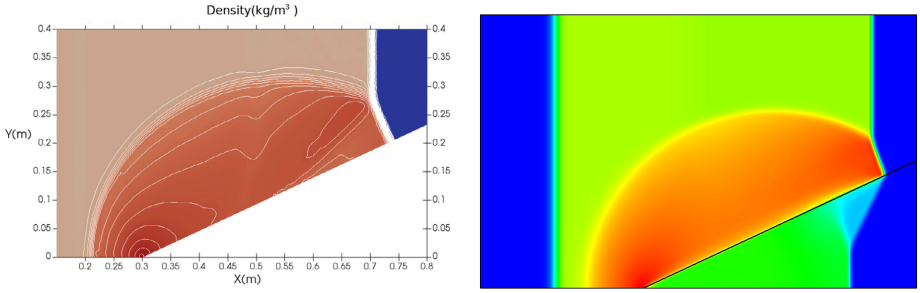

(a) Xiao *et al.* (2017) (b) Present work

Figure 7. Specific mass field.

3.3 Supersonic flow on an ascending step

This case was based on the work of Woodward and Colella (1984). The figure(8) presents a scheme of the problem, which starts with a uniform flow with Mach number $Ma = 3$. The entrance is on the left and the outlet on the right of the domain. Initially, the field is filled by a perfect gas with the relation between specific heats at constant pressure and volume of 1.4 , pressure $p = 1$, specific mass $\rho = 1.4$, and velocity with the components $u = 3$ and $v = 0$. The inlet is continuously supplied with gas presenting these values of pressure, specific mass, and velocity. Along the walls, top, and bottom of the domain, impermeable wall boundary conditions and slip conditions are applied. The step was modeled with an immersed boundary.

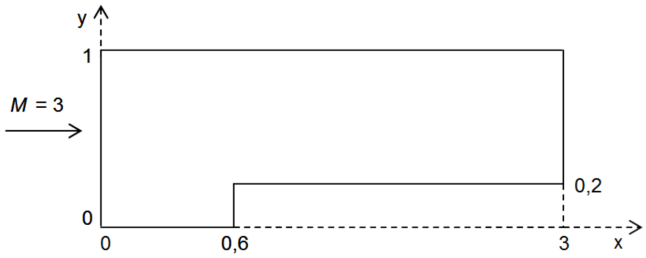

Figure 8. Setup of the supersonic flow over an ascending step.

The figure (9) presents the temporal evolution of the supersonic flow. The transient solution was also adequately represented. A qualitative comparison was made in relation to the results given by the cited reference. The specific mass fields are similar to those obtained by the authors. Reflections of the shock waves on the step, the top wall, and the bottom wall were consistently captured.

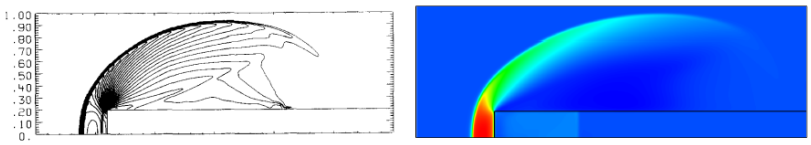

(a) Instant 1

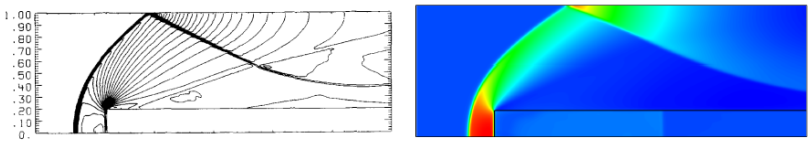

(b) Instant 2

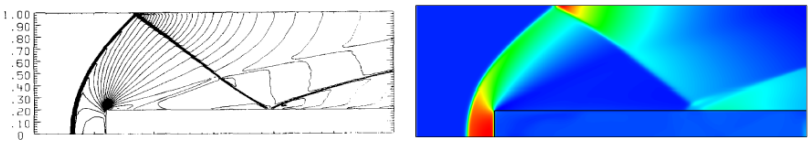

(c) Instant 3

Figure 9. Specific mass at different times for the case of supersonic flow on an ascending step

Next, validation results for a curved geometry will be presented, a cylinder immersed in a supersonic flow.

3.4 Supersonic flow over a cylinder

To simulate the supersonic flow over a cylinder, a configuration based on the work of Burbeau and Sagaut (2002) was set. The problem considered is a supersonic flow that passes through a circular cylinder in a free stream with a Reynolds number of $Re = 100$. The Reynolds number is defined as $Re = DU/\nu$, where D is the cylinder diameter, U is the free stream velocity, and ν is the kinematic viscosity. In the present simulation D is set as 0.1, U is set as unitary, and consequently $\nu = 0.001$. The computational domain is illustrated in the figure (10). The initial conditions were defined as: $\rho = 1$, $u = 1$, $v = 0$, $P = \frac{1}{\gamma M_O^2}$, $\gamma = 1.4$ and the Mach number in the input was set to $M_O = 2$.

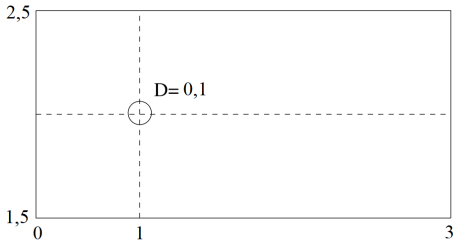

Figure 10. Setup of the case of supersonic flow over a cylinder.

The Figure (11) presents a comparison of the specific mass field with the result of Burbeau and Sagaut (2002). There is a remarkable similarity in the results, the formation of the shock wave upstream of the cylinder, the downstream region, from the central area, and in the waves reflected along the domain.

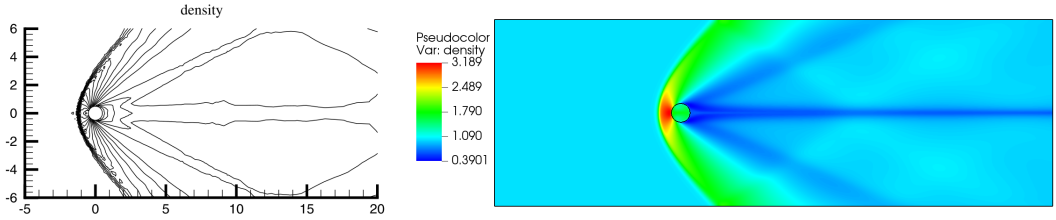

(a) Burbeau and Sagaut (2002) (b) Present

Figure 11. Specific mass field.

The Figure (12) presents a comparison of the Mach number field with the result of Burbeau and Sagaut (2002). As in the previous figure, there is a remarkable similarity between the solution and the reference result, reducing the Mach number in the shock wave and the central region downstream of the cylinder.

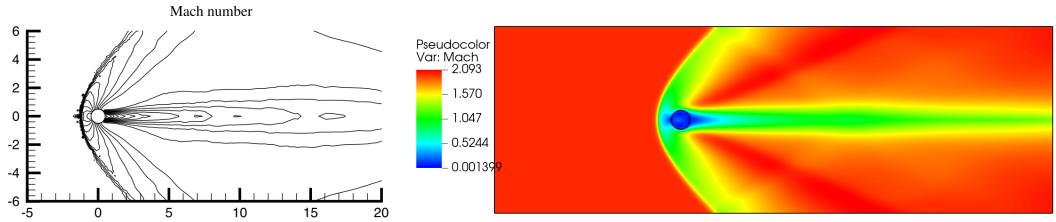

(a) Burbeau and Sagaut (2002) (b) Present

Figure 12. Mach field.

To quantitatively validate, a turbulent case was simulated with the Reynolds number $Re = 2.0 \cdot 10^5$ and Mach number $Ma = 1.7$. This case was based on the work of Palma *et al.* (2006). For the turbulence modeling, the Spalart-Allmaras model (Spalart and Allmaras, 1992) was used, which is already implemented in MFSim code. The Figure (13) presents the comparison of the Mach field obtained with Palma *et al.* (2006). There is a similarity between the two results, from the shock wave formation to the region of low Mach that forms downstream of the cylinder.

The Figure (14) shows the evolution of the drag coefficient C_D as a function of time. We note that for the initial times, approximately $t = 0.3$ and $t = 0.4$, there is numerical oscillation due to the reflection waves from the imposition of zero velocity across the immersed boundary. Due to the reflections in the complementary region inside the cylinder, there is an alteration in the lagrangian force (force at the immersed boundary), causing this numerical oscillation in the drag coefficient. After $t = 0.5$, a physical instability is observed, resulting from the flow characteristic. With the time evolution, the drag coefficient converges to 1.6.

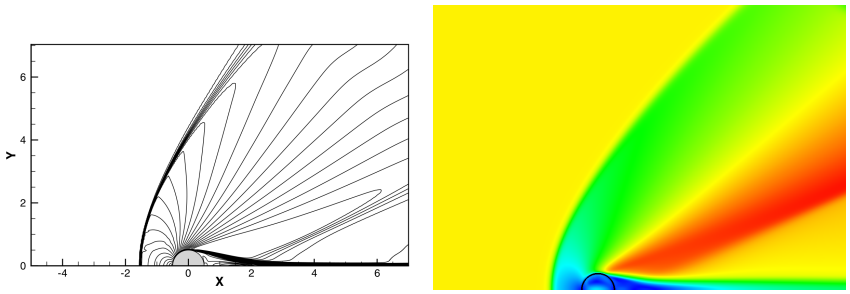

(a) Palma *et al.* (2006) (b) Present

Figure 13. Mach number fields for the turbulent case.

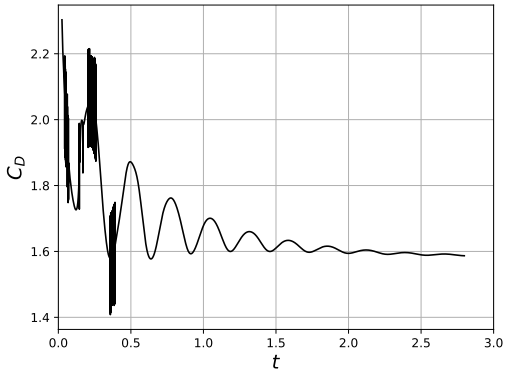

Figure 14. Temporal evolution of the drag coefficient.

The Table (1) presents a comparison between the drag coefficient obtained through the numerical solution and experimental data from Bashkin *et al.* (2002) and numerical data from Palma *et al.* (2006). We observed a relative difference of 11.19% between the obtained and the experimental, which is considered satisfactory considering the complexity of the solution (high Mach and Reynolds numbers).

Table 1. Comparison of the drag coefficients.

	Cd	Relative Difference
Bashkin et al. (Physical experiment)	1,43	**
Palma et al. (Numerical experiment)	1,39	2,80%
Present work	1,59	11,19%

The Table (2) presents the angle of the point of detachment, also compared with the references Bashkin *et al.* (2002); Palma *et al.* (2006). We observed a relative difference of 10.71% between the obtained solution and the experimental data, which is also considered satisfactory.

Table 2. Comparison of the point of detachment

	Point of detachment [^{o}]	Relative Difference
Bashkin et al. (Physical experiment)	112	**
Palma et al. (Numerical experiment)	111	0,89%
Present work	124	10,71%

4. CONCLUSION

This present work presents the numerical experiments of compressible flow using the immersed boundary method with the multi direct forcing technic. Cartesian numerical meshes are used for non-Cartesian problems thanks to the dynamic immersed boundary method. Satisfactory results were obtained for the benchmark test cases, showing a good efficiency of the applied technique.

5. ACKNOWLEDGEMENTS

The authors gratefully acknowledge financial support from PETROBRAS, CEFET-MG, Capes, CNPQ and Fapemig. The authors are also grateful to the mechanical engineering graduate program from the Federal University of Uberlândia (UFU).

6. REFERENCES

Bashkin, V., Vaganov, A., Egorov, I., Ivanov, D. and Ignatova, G., 2002. "Comparison of calculated and experimental data on supersonic flow past a circular cylinder". *Fluid dynamics*, Vol. 37, No. 3, pp. 473–483.

Burbeau, A. and Sagaut, P., 2002. "Simulation of a viscous compressible flow past a circular cylinder with high-order discontinuous galerkin methods". *Computers e Fluids*, Vol. 31, No. 8, pp. 867 – 889. ISSN 0045-7930. doi:https://doi.org/10.1016/S0045-7930(01)00055-X. URL http://www.sciencedirect.com/science/article/pii/S004579300100055X.

Darwish, M. and Moukalled, F., 2014. "A fully coupled navier-stokes solver for fluid flow at all speeds". *Numerical Heat Transfer, Part B: Fundamentals*, Vol. 65, No. 5, pp. 410–444.

Darwish, M., Sraj, I. and Moukalled, F., 2007. "A coupled incompressible flow solver on structured grids". *Numerical Heat Transfer, Part B: Fundamentals*, Vol. 52, No. 4, pp. 353–371.

Darwish, F Moukalled, M., 2000. "A unified formulation of the segregated class of algorithms for fluid flow at all speeds". *Numerical Heat Transfer: Part B: Fundamentals*, Vol. 37, No. 1, pp. 103–139.

Darwish, M., Sraj, I. and Moukalled, F., 2009. "A coupled finite volume solver for the solution of incompressible flows on unstructured grids". *Journal of Computational Physics*, Vol. 228, No. 1, pp. 180–201.

Ferziger, J.H. and Peric, M., 2012. *Computational methods for fluid dynamics*. Springer Science & Business Media.

Harlow, F.H. and Amsden, A.A., 1968. "Numerical calculation of almost incompressible flow". *Journal of Computational Physics*, Vol. 3, No. 1, pp. 80–93.

Maliska, C., 1995. *Transferência de Calor e Mecânica dos Fluídos Computacional*. LTC.

Melo, R.R.S., Kinoshita, D., Villar, M.M., Serfaty, R. and da Silveira Neto, A., 2020. "Numerical experiment of turbulent transfer of thermal energy using the immersed boundary method and adaptive mesh refinement". *International Journal of Thermal Sciences*, Vol. 151, p. 106281. ISSN 1290-0729. doi:https://doi.org/10.1016/j.ijthermalsci.2020.106281. URL https://www.sciencedirect.com/science/article/pii/S1290072919304260.

Palma, P.D., de Tullio, M., Pascazio, G. and Napolitano, M., 2006. "An immersed-boundary method for compressible viscous flows". *Computers & Fluids*, Vol. 35, No. 7, pp. 693 – 702. ISSN 0045-7930. doi:https://doi.org/10.1016/j.compfluid.2006.01.004. URL http://www.sciencedirect.com/science/article/pii/S0045793006000065. Special Issue Dedicated to Professor Stanley G. Rubin on the Occasion of his 65th Birthday.

Patankar, S.V. and Spalding, D.B., 1983. "A calculation procedure for heat, mass and momentum transfer in three-dimensional parabolic flows". In *Numerical Prediction of Flow, Heat Transfer, Turbulence and Combustion*, Elsevier, pp. 54–73.

Spalart, P.R. and Allmaras, S.R., 1992. "A one-equation turbulence model for aerodynamic flows". *AIAA Paper*.

Wang, Z., Fan, J. and Luo, K., 2008. "Combined multi direct forcing immersed boundary method for simulating flows with moving particles". *International Journal of Multiphase Flow*.

Woodward, P. and Colella, P., 1984. "The numerical simulation of two-dimensional fluid flow with strong shocks". *Journal of Computational Physics*, Vol. 54, No. 1, pp. 115 – 173. ISSN 0021-9991. doi:https://doi.org/10.1016/0021-9991(84)90142-6. URL http://www.sciencedirect.com/science/article/pii/0021999184901426.

Xiao, C.N., Denner, F. and van Wachem, B.G., 2017. "Fully-coupled pressure-based finite-volume framework for the simulation of fluid flows at all speeds in complex geometries". *Journal of Computational Physics*, Vol. 346, pp. 91 – 130. ISSN 0021-9991. doi:https://doi.org/10.1016/j.jcp.2017.06.009. URL http://www.sciencedirect.com/science/article/pii/S0021999117304540.

7. RESPONSIBILITY NOTICE

The authors are solely responsible for the printed material included in this paper.